

# Sliding DFT-based Signal Recovery for Modulo ADC with 1-bit Folding Information

Neil Irwin Bernardo, *Member, IEEE*

**Abstract**—The modulo analog-to-digital converter (ADC) is a promising solution to resolve the limited dynamic range (DR) issue of conventional ADCs. However, a modulo ADC requires an unfolding scheme to correct the nonlinear distortion introduced by the modulo operation. This paper presents a sliding discrete Fourier Transform (DFT)-based method for fast signal reconstruction given the modulo ADC output sequence and a 1-bit folding information sequence. In contrast to existing DFT-based signal recovery techniques for modulo ADCs, our proposed sliding DFT method reduces the required observation time and minimizes the spectral leakage effects via proper choice of window function parameters. A mean squared error (MSE) performance guarantee is established for the proposed signal recovery algorithm. More precisely, we derive sufficient conditions for the oversampling factor (OF) and the number of quantization bits ( $b$ ) to obtain a specific MSE performance. Our numerical results demonstrate that modulo ADCs equipped with our proposed recovery method can outperform conventional ADCs without modulo for  $OF \geq 4$  and  $b \geq 4$ . The impact of spectral leakage on the MSE performance of the proposed sliding DFT recovery method is also quantified.

**Index Terms**—Modulo ADC, Sampling, Quantization, DFT.

## I. INTRODUCTION

An analog-to-digital converter (ADC) is a critical element of data acquisition systems since it is responsible for the transformation of continuous-time analog observations from the physical world into some format that can be further processed or stored in digital signal processing (DSP) pipelines. The conversion process in conventional ADCs involves two operations: (1) a *sampler* that acquires the amplitude of the continuous-time input at uniform time intervals, and (2) a *quantizer* that maps the amplitude samples into a finite set of discrete values [1]. The sampling rate and quantizer resolution of an ADC are chosen according to some fidelity criterion and power consumption budget. Theoretically, the sampling rate requirement for alias-free reconstruction and the quantization resolution needed to achieve some distortion level are governed by the Shannon-Nyquist sampling theorem [2] and the rate-distortion theory [3], respectively. However, increasing these parameters also incurs a substantial increase in the ADC power consumption. More precisely, the ADC power consumption scales exponentially with the number of quantization bits and scales linearly with the sampling rate [4].

Another important parameter that affects the performance of an ADC is the dynamic range (DR). Due to the finite number of quantization bits in an ADC, a trade-off exists between its dynamic range and its resolution. An input signal may

drive the ADC into saturation if the DR of the input signal far exceeds the DR of the ADC. However, increasing the ADC range to accommodate high DR signals would increase the quantization step size. Weak input signals could be buried in the quantization noise. The presence of both weak and strong components in the input signal increases the required ADC resolution to achieve a specific fidelity criterion [5].

A promising solution to address the DR bottleneck of ADCs is the *modulo sampling* framework [6]. The idea in modulo sampling is to apply a nonlinear folding operation called *modulo* to the input signal before the ADC. This modulo preprocessing stage ensures that the signal range is confined within the DR of the ADC. Since modulo operation intentionally introduces nonlinear distortion to the signal, several studies on modulo sampling have focused on the development of robust recovery techniques to correct the distortion induced by the modulo operation. Reconstruction techniques for modulo sampling include higher-order differences-based approaches [6], discrete Fourier transform (DFT)-based techniques [7]–[11], prediction-based filtering [12], iterative methods [13], sparse signal modulo recovery [14]–[16], and dual-channel modulo structures [17]. There are also research efforts geared toward the practical hardware implementation of modulo ADCs [18]–[20] and their potential applications in radars, communication systems, imaging, and electroencephalogram (EEG) recovery [17], [21]–[28].

Another important research direction in modulo ADC is the establishment of theoretical performance guarantees to reconstruct the unfolded signal from modulo samples. In [6], it is shown that the higher-order differences-based reconstruction approach can perfectly reconstruct a finite-energy bandlimited (BL) signal from its modulo samples if the sampling rate used is at least  $2\pi e$  ( $\approx 17.07$ ) times the Nyquist rate. This sufficient condition for the sampling rate increases significantly in the presence of bounded noise [6, Theorem 3]. For finite-energy BL signals, perfect reconstruction is possible for any sampling rate approaching the Nyquist rate from above by using a prediction filter with sufficiently long filter length [20]. However, the proposed approach did not take into account the impact of finite quantization. Theoretical guarantees for Fourier-based reconstruction had been established in [7]. However, this approach suffers from spectral leakage and may require long observation windows. A recent work on modulo ADCs with 1-bit side information [10] established a mean squared error (MSE) performance guarantee when the oversampling factor (OF) is above three and the number of quantization bits is above three. The 1-bit side information identifies the indices in which folding occurred. However, the proofs neglected the spectral leakage effects and the contribution of quantization

N.I. Bernardo is with the Electrical and Electronics Engineering Institute, University of the Philippines Diliman, Quezon City 1101, Philippines (e-mail: neil.bernardo@eee.upd.edu.ph).

noise at certain time indices.

In this work, we propose a sliding DFT approach to construct the original input samples from the modulo ADC output samples and an additional 1-bit folding information signal. The recovery procedure uses short-time Fourier transform (STFT) to facilitate successive frame-based unfolding of the modulo samples. To significantly reduce the impact of spectral leakage in STFT computation, windowing is incorporated in the recovery method. A MSE performance guarantee for the proposed recovery method is also established and is compared with the simulated MSE results.

The main contributions of this work are summarized as follows:

- We develop an unfolding algorithm for modulo ADC output with 1-bit folding information signal based on sliding-window DFT. In contrast to existing Fourier-based reconstruction techniques, the proposed algorithm does not need a long observation window to process the modulo ADC output. This significantly reduces the computational complexity of the recovery algorithm. Furthermore, spectral leakage due to the short frame observations can be reduced by choosing an appropriate window function.
- We establish sufficient conditions for the oversampling factor (OF) and quantizer resolution of the modulo ADC so that the proposed recovery algorithm can correctly unfold the modulo ADC output. Under these conditions, the MSE performance of the sliding DFT recovery algorithm is derived (see Theorem 1).
- We compare the MSE of the modulo ADC equipped with our proposed recovery procedure to that of the conventional ADC, i.e., no modulo operation. Under the established sufficient conditions, we show that the MSE of the modulo ADC which uses the sliding DFT recovery algorithm is in  $\mathcal{O}\left(\frac{1}{\text{OF}^3}\right)$  when spectral leakage is neglected and is in  $\mathcal{O}\left(\frac{1}{\text{OF}^2}\right)$  otherwise. The parameter OF is the oversampling factor to be defined in Section II. Meanwhile, the MSE of a conventional ADC is in  $\mathcal{O}\left(\frac{1}{\text{OF}}\right)$ . Numerical results are presented to demonstrate these behaviors.

*Notation:* The following notations are used throughout the paper. The sets of real numbers, integers, and natural numbers are denoted as  $\mathbb{R}$ ,  $\mathbb{Z}$ , and  $\mathbb{N}$ , respectively. When referring to discrete-time signals, the notation  $z[n]$  is used to signify  $z(nT_s)$ , assuming that the sampling period  $T_s$  is evident from the context. The first-order difference of a discrete-time signal  $x[n]$  is denoted as  $\underline{x}[n] = x[n] - x[n-1]$ , where  $x[-1] = 0$  unless stated otherwise. Vectors and matrices are written in bold format (e.g.,  $\mathbf{z}$ ,  $\mathbf{A}$ ) while sets are written in calligraphic format (e.g.,  $\mathcal{S}$ ). If  $\mathbf{x}$  is a vectorized form of some discrete-time signal  $x[n]$ , then  $\underline{\mathbf{x}}$  is the vectorized form of  $\underline{x}[n]$ . The  $\ell_p$ -norm of a vector  $\mathbf{x}$  is written as  $\|\mathbf{x}\|_p$ . The set of values of the discrete-time signal  $x[n]$  for  $n \in \mathcal{S}$  is denoted as  $x_{\mathcal{S}}[n]$ . The Moore-Penrose inverse of a matrix  $\mathbf{A} \in \mathbb{R}^{m \times n}$  is denoted by  $\mathbf{A}^\dagger$ . We also use the standard Big-O notation  $\mathcal{O}(\cdot)$  to describe asymptotic growth rates in this paper.

## II. SYSTEM MODEL AND RECONSTRUCTION ALGORITHM

### A. Signal Acquisition Process

We consider the modulo ADC system shown in Figure 1. The input  $f(t)$  is a bandlimited signal with (angular) frequency support  $\left[-\frac{\omega_m}{2}, +\frac{\omega_m}{2}\right]$ . This signal is folded by the modulo operator block to produce the modulo signal  $f_{\lambda'}(t)$ . The operation behind the modulo folding mechanism is shown in Figure 2. This feedback structure for the folding operation is adopted from [18]. Comparator 1 triggers a positive value whenever  $f_{\lambda'}(t)$  crosses  $+\lambda$  from below. Similarly, comparator 2 triggers a negative value whenever  $f_{\lambda'}(t)$  crosses  $-\lambda$  from above. These trigger signals are fed to a discrete voltage generator (DVG). The voltage level of the DVG is increased (resp. decreased) by  $2\lambda'$  whenever it receives a positive (resp. negative) trigger signal. A detailed circuit-level implementation of the DVG is presented in [18]. Mathematically, the folded signal can be expressed as

$$f_{\lambda'}(t) = \left[ (f(t) + \lambda') \bmod 2\lambda' \right] - \lambda', \quad (1)$$

where  $\lambda' \in (0, \|f(t)\|_\infty)$  is the modulo threshold. The  $\ell_\infty$ -norm of a waveform is its maximum amplitude.

To digitize the modulo signal,  $f_{\lambda'}(t)$  is first sampled at every  $T_s$  seconds. The angular sampling rate is  $\omega_s = \frac{2\pi}{T_s} = \text{OF} \times \omega_m$ , where  $\text{OF} \geq 1$  is the oversampling factor. We also define  $\rho = \frac{1}{\text{OF}}$ . Prior to quantization, a (non-subtractive) dither sequence  $d[n]$  is added to  $f_{\lambda'}[n]$ . Samples of the dither sequence are drawn i.i.d. from a triangle distribution with amplitude support  $\left(-\frac{2\lambda}{2^b}, +\frac{2\lambda}{2^b}\right)$ . The rationale for using triangle dither in the modulo ADC problem setup is explained in Section III-B. The resulting signal is then forwarded to the  $b$ -bit uniform scalar quantizer  $\mathcal{Q}_b(\cdot)$  with range  $[-\lambda, +\lambda]$ . Consequently, each quantization bin has width  $\frac{2\lambda}{2^b}$ . To prevent the quantizer from being overloaded, the modulo threshold is set to  $\lambda' = \frac{(2^b - 2)\lambda}{2^b}$ . The quantizer output can be written as

$$\begin{aligned} f_{\lambda',q}[n] &= \mathcal{Q}_b(f_{\lambda'}[n] + d[n]) \\ &= f[n] + z[n] + \epsilon[n], \end{aligned} \quad (2)$$

where  $z[n] = f_{\lambda'}[n] - f[n] \in 2\lambda'\mathbb{Z}$  is the residual samples due to the folding operation and  $\epsilon[n] = \mathcal{Q}_b(f_{\lambda'}[n] + d[n]) - f_{\lambda'}[n]$  is the quantization noise sequence.

In addition to  $f_{\lambda'}(t)$ , the modulo operator also generates a 2-level signal  $c(t)$  according to Figure 2. This signal is a finite rate of innovation (FRI) signal and can be expressed as

$$c(t) = g_2(t) * \left( \sum_k g_1(t - \tau_k) \right) = \sum_k g(t - \tau_k),$$

where  $\tau_k$  is the location of the level crossings,  $g_1(t)$  is the pulse shape of the trigger signals,  $g_2(t)$  is the sampling kernel, and  $g(t) = (g_2 * g_1)(t)$ . To simplify the analysis,  $g(t)$  is assumed to be a rectangular pulse with width  $T_s$  and unity amplitude. The signal  $c(t)$  is sampled at rate  $\omega_s$  and then fed to a 1-bit comparator to produce  $c[n]$ . In essence,  $c[n]$  provides information if the signal crossed either  $+\lambda'$  or  $-\lambda'$  in the interval  $(nT_s, (n+1)T_s]$ .

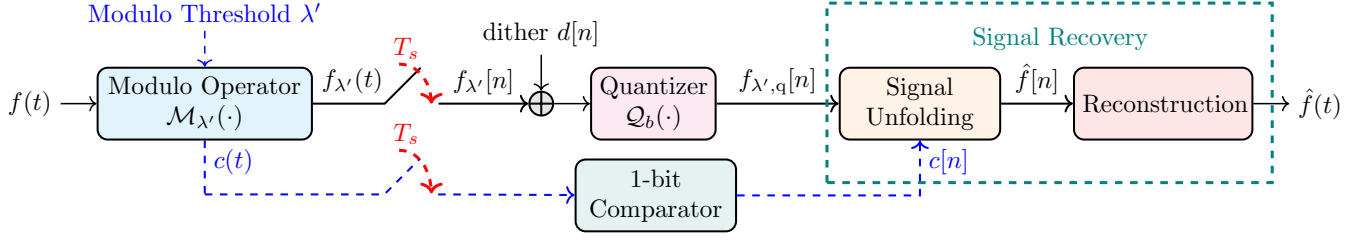


Fig. 1. The schematic diagram of the modulo ADC with 1-bit side information. The 1-bit level crossing information  $c[n]$  is obtained by sampling  $c(t)$ .

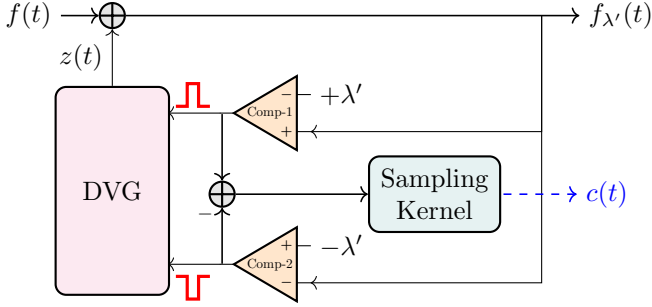


Fig. 2. The folding mechanism and side information generation of the modulo operator block.

### B. Is the 1-bit Folding Information Practical?

One might wonder if generating 1-bit folding information  $c[n]$  is practical when implementing a modulo ADC. Early works on modulo ADC hardware have considered recovery methods that utilize the reset count in addition to the modulo samples [29], [30]. However, implementing a modulo ADC with a multi-bit reset count signal may incur a significant increase in power consumption and circuit complexity if the modulo threshold is small [6]. Limiting  $c[n]$  to 1-bit solves these problems. As shown in Figures 1 and 2, generating  $c[n]$  would only require one additional comparator and one adder from the “no  $c[n]$ ” modulo ADC setup. The additional circuitry has minimal impact on the overall power consumption, and its penalty is fixed regardless of  $b$ . For instance, an 8-bit modulo ADC with no  $c[n]$  would have  $2^8 + 2 = 258$  comparators<sup>1</sup> whereas an 8-bit modulo ADC with 1-bit folding information  $c[n]$  would have 259 comparators. We also note that the folding information generated in Figure 1 is one bit less than the folding information generated by the modulo ADC hardware proposed in [19]<sup>2</sup>.

### C. Signal Recovery Scheme

The proposed recovery algorithm first unfolds  $f_{\lambda',q}[n]$  by estimating  $z[n]$  and then reconstructs the continuous-time signal from the result. Since the sampling frequency used is above the Nyquist rate, the continuous-time signal can be uniquely identified using an appropriate reconstruction filter. In this subsection, we discuss the unfolding mechanism. An overview

of the proposed unfolding procedure is given in Figure 3. The unfolding scheme multiplies a window signal  $w[n]$  to small overlapping segments of  $f_{\lambda',q}[n]$  and then recovers the modulo residue signal at each segment. The window is slid from left to right until the whole  $f_{\lambda',q}[n]$  is processed.

Let  $N$  be the number of samples in a short segment of  $f_{\lambda',q}[n]$ . A length- $N$  tapered cosine window  $w[n]$  (a.k.a. Tukey window [31]) can be written as

$$w[n] = \begin{cases} \frac{1 + \cos\left(\frac{2\pi}{\alpha}\left(\frac{n}{N} - \frac{\alpha}{2}\right)\right)}{2}, & 0 \leq n < \frac{\alpha N}{2} \\ 1, & \frac{\alpha N}{2} \leq n < N\left(1 - \frac{\alpha}{2}\right) \\ \frac{1 + \cos\left(\frac{2\pi}{\alpha}\left(\frac{n}{N} - 1 + \frac{\alpha}{2}\right)\right)}{2}, & N\left(1 - \frac{\alpha}{2}\right) \leq n < N \end{cases},$$

where the parameter  $\alpha > 0$  is the roll-off factor. We choose  $\alpha$  so that  $\alpha N \in 2\mathbb{Z}$ .

Suppose the  $i$ -th segment of  $f_{\lambda',q}[n]$  is denoted as  $f_{\lambda',q}^{(i)}[n]$  and the  $i$ -th segment of the unfolded signal as  $f^{(i)}[n]$ . Consecutive segments overlap such that the last  $\frac{\alpha N}{2}$  samples of  $f_{\lambda',q}^{(i-1)}[n]$  are the first  $\frac{\alpha N}{2}$  samples of  $f_{\lambda',q}^{(i)}[n]$ . The window function  $w[n]$  is multiplied to the first-order difference of  $f_{\lambda',q}[n]$  to get

$$\begin{aligned} \tilde{f}_w^{(i)}[n] &= w[n] \cdot \underline{f}_{\lambda',q}^{(i)}[n] \\ &= w[n] \cdot \left( f_{\lambda',q}^{(i)}[n] - f_{\lambda',q}^{(i)}[n-1] \right). \end{aligned} \quad (3)$$

We now describe the computation of the modulo residue samples in  $f_{\lambda',q}^{(i)}[n]$ . The length- $N$  Discrete Fourier Transform (DFT) of  $\tilde{f}_w^{(i)}[n]$  is computed as

$$\hat{F}_w(e^{j\frac{2\pi k}{N}}) = \frac{1}{\sqrt{N}} \sum_{n=0}^{N-1} \tilde{f}_w^{(i)}[n] e^{-j\frac{2\pi kn}{N}}. \quad (4)$$

Due to the finite bandwidth assumption on  $f(t)$ ,  $\hat{F}_w(e^{j\frac{2\pi kn}{N}})$  for  $\frac{2\pi k}{N} \in (\rho\pi + \Omega_{SL}, 2\pi - \rho\pi - \Omega_{SL})$  can be written as

$$\begin{aligned} \hat{F}_{\text{OOB}}(e^{j\frac{2\pi k}{N}}) &= \frac{1}{\sqrt{N}} \sum_{n=0}^{L-1} w[n] \left[ \underline{z}^{(i)}[n] + \underline{\epsilon}^{(i)}[n] \right] e^{-j\frac{2\pi kn}{N}} \\ &= \frac{1}{\sqrt{N}} \sum_{n \in \mathcal{S}_i} w[n] \left[ \underline{z}_{\mathcal{S}_i}^{(i)}[n] + \underline{\epsilon}_{\mathcal{S}_i}^{(i)}[n] \right] e^{-j\frac{2\pi kn}{N}} \\ &\quad + \frac{1}{\sqrt{N}} \sum_{n \notin \mathcal{S}_i} w[n] \cdot \underline{\epsilon}_{\mathcal{S}_i}^{(i)}[n] \cdot e^{-j\frac{2\pi kn}{N}}, \end{aligned} \quad (5)$$

where the spectral leakage width, denoted  $\Omega_{SL}$ , accounts for the frequencies where spectral leakage is still significant. Some energy of the  $\tilde{f}_w^{(i)}[n]$  may leak in the band  $(\rho\pi, 2\pi - \rho\pi)$  due to the inherent spectral leakage in the DFT computation

<sup>1</sup>The 2 additional comparators come from the comparators of the folding mechanism.

<sup>2</sup>In [19], the 2-bit signal indicates three states: ‘no crossing’, ‘crossed  $+\lambda'$  threshold’, ‘crossed  $-\lambda'$  threshold’.

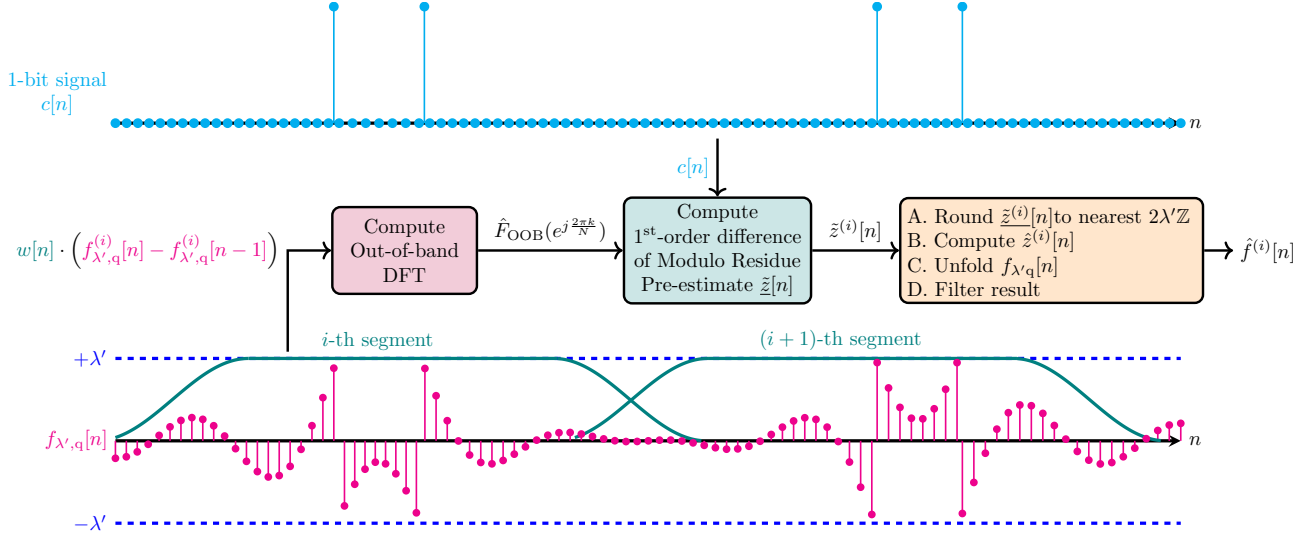


Fig. 3. Overview of the proposed sliding DFT-based unfolding method for modulo sampling.

and cannot be neglected. However, spectral leakage can be controlled by properly choosing the window length  $N$  and roll-off parameter  $\alpha$ . The signals  $z^{(i)}[n]$  and  $\epsilon^{(i)}[n]$  are the first-order difference of the modulo residue samples and quantization noise, respectively, in the  $\hat{f}_w^{(i)}[n]$ . The set  $\mathcal{S}_i$  contains the indices for which  $c[n] = 1$  in the  $i$ -th segment. The set identifies the indices in the  $i$ -th segment for which the DVG changes its output voltage. The samples  $z_{\mathcal{S}_i}^{(i)}[n]$  (resp.  $z_{\mathcal{S}_i^c}^{(i)}[n]$ ) corresponds to the value of the modulo residue for all  $n$  such that  $c[n] = 1$  (resp.  $c[n] = 0$ ) in the  $i$ -th segment. The subscript OOB in  $\hat{F}_{\text{OOB}}$  is used to indicate that this is the set of DFT coefficients outside the desired signal bandwidth plus non-negligible spectral leakage.

We are primarily interested in estimating  $z_{\mathcal{S}_i}^{(i)}[n]$ . Let  $K$  be the number of discrete frequencies  $k$  such that  $\frac{2\pi k}{N} \in (\rho\pi + \Omega_{\text{SL}}, 2\pi - \rho\pi - \Omega_{\text{SL}})$ . Equation (5) can be written in matrix form as

$$\hat{\mathbf{F}}_{\text{OOB}} = \mathbf{V}(\mathbf{z}_w + \boldsymbol{\epsilon}_w), \quad (6)$$

where  $\mathbf{z}_w \in \mathbb{R}^{N \times 1}$ ,  $\boldsymbol{\epsilon}_w \in \mathbb{R}^{N \times 1}$ , and  $\hat{\mathbf{F}}_{\text{OOB}} \in \mathbb{C}^{K \times 1}$  are vectorized form of the finite-length signals  $w[n] \cdot z^{(i)}[n]$ ,  $w[n] \cdot \epsilon^{(i)}[n]$ , and  $\hat{F}_{\text{OOB}}(e^{j\frac{2\pi k}{N}})$ , respectively. The entry of matrix  $\mathbf{V} \in \mathbb{C}^{K \times N}$  in the  $k'$ -th row and  $n$ -th column is  $e^{-j\frac{2\pi n k'}{N}}$ , where  $\frac{2\pi k'}{N}$  is the  $k'$ -th discrete frequency in  $(\rho\pi + \Omega_{\text{SL}}, 2\pi - \rho\pi - \Omega_{\text{SL}})$ . Let  $\mathbf{z}_{w, \mathcal{S}_i} \in \mathbb{R}^{|\mathcal{S}_i| \times 1}$  and  $\boldsymbol{\epsilon}_{w, \mathcal{S}_i} \in \mathbb{R}^{|\mathcal{S}_i| \times 1}$  contain the elements of  $\mathbf{z}_w$  and  $\boldsymbol{\epsilon}_w$  whose indices  $n \in \mathcal{S}_i$ . Then, a pre-estimate of  $\mathbf{z}_{w, \mathcal{S}_i}$ , denoted as  $\hat{\mathbf{z}}_{w, \mathcal{S}_i}$ , can be expressed as

$$\hat{\mathbf{z}}_{w, \mathcal{S}_i} = \mathbf{V}_{\mathcal{S}_i}^\dagger \hat{\mathbf{F}}_{\text{OOB}}, \quad (7)$$

where  $\mathbf{V}_{\mathcal{S}_i} \in \mathbb{C}^{K \times |\mathcal{S}_i|}$  is formed by horizontally stacking the columns of  $\mathbf{V}$  whose column indices are in  $\mathcal{S}_i$ . We obtain the (windowed) pre-estimate of  $z^{(i)}[n]$ , denoted  $\hat{z}_w^{(i)}[n]$ , by placing the corresponding values of  $\hat{\mathbf{z}}_{w, \mathcal{S}_i}$  to  $\hat{z}_w^{(i)}[n]$  for  $n \in \mathcal{S}_i$ . The values of  $\hat{z}_w^{(i)}[n]$  for  $n \notin \mathcal{S}_i$  are set to 0.

Note that the  $n$ -th element of  $\hat{z}_w^{(i)}[n]$  for  $n \in \{0, \dots, \frac{\alpha N}{2}\}$  has a non-unity scaling of the desired modulo residue signal

$z^{(i)}[n]$  due to the tapered cosine window  $w[n]$ . To correct this scaling, we exploit the symmetry of the window function at the edges:

$$w[n] + w[n + N(1 - \frac{\alpha}{2})] = 1 \quad \forall n \in \{0, 1, \dots, \frac{\alpha N}{2} - 1\}. \quad (8)$$

We take the last  $\frac{\alpha N}{2}$  samples of  $\hat{z}_w^{(i-1)}[n]$  and add them to the first  $\frac{\alpha N}{2}$  samples of  $\hat{z}_w^{(i)}[n]$ <sup>3</sup>. The resulting signal is

$$\hat{z}^{(i)}[n] = \begin{cases} \hat{z}_w^{(i)}[n] + \hat{z}_w^{(i-1)}[n + N(1 - \frac{\alpha}{2})], & 0 \leq n < \frac{\alpha N}{2} \\ \hat{z}_w^{(i)}[n], & \frac{\alpha N}{2} \leq n < N(1 - \frac{\alpha}{2}) \end{cases}$$

Since  $z^{(i)}[n] \in 2\lambda'\mathbb{Z}$ ,  $\hat{z}^{(i)}[n] \in 2\lambda'\mathbb{Z}$ . The samples of the first-order difference of modulo residue pre-estimates  $\hat{z}^{(i)}[n]$  are rounded to the nearest integer multiple of  $2\lambda'$  to get the first-order difference of the modulo residue estimates, denoted as  $\hat{z}^{(i)}[n]$ . To undo the first-order difference operation in the modulo residue signal, the formula

$$\hat{z}^{(i)}[n] = \hat{z}^{(i-1)}[n] + \hat{z}^{(i)}[n] \quad (9)$$

is applied. The modulo residue signal estimate  $\hat{z}^{(i)}[n]$  is then subtracted from  $f_{\lambda',q}^{(i)}[n]$  to unfold the  $i$ -th segment for  $n \in \{0, \dots, N(1 - \frac{\alpha N}{2})\}$ . Finally, a digital lowpass filter with passband region  $(-\frac{\Omega_m}{2} - \Omega_{\text{SL}}, +\frac{\Omega_m}{2} + \Omega_{\text{SL}})$  is applied to the result, where  $\Omega_m = \omega_m T_s$ . The unfolded signal can be expressed as

$$\begin{aligned} \hat{f}^{(i)}[n] &= \left\{ f_{\lambda',q}^{(i)}[n] - \hat{z}^{(i)}[n] \right\}_{\text{LPF}} \\ &= f^{(i)}[n] + \left\{ z^{(i)}[n] - \hat{z}^{(i)}[n] \right\}_{\text{LPF}} + \epsilon_{\text{LPF}}^{(i)}[n] \end{aligned} \quad (10)$$

for  $n \in \{0, \dots, N(1 - \frac{\alpha N}{2})\}$ . The subscript LPF is used to indicate that the modulo residue error signal and quantization noise signal were filtered. The recovery procedure continues until all segments of  $f_{\lambda',q}[n]$  have been processed.

<sup>3</sup>Due to the sliding window approach,  $\hat{z}_w^{(i-1)}[n]$  is already available when processing the  $i$ -th segment of  $f_{\lambda',q}[n]$

### D. Proposed Recovery Scheme vs. Other DFT-based Techniques

Due to the DFT computation, our proposed recovery scheme can be classified as a DFT-based recovery technique. Other algorithms under this category are the Fourier-Prony method [7],  $B^2R^2$  [8], and LASSO- $B^2R^2$  [9]. The advantage of our proposed recovery scheme is that it does not restrict the signal to decay over time (such as in  $B^2R^2$  and LASSO- $B^2R^2$ ) nor does it require the signal to be periodic (such as in Fourier-Prony method). The window function ensures that sharp discontinuities are avoided at the periodic boundaries when the length- $N$  sampled signal is repeated. Consequently, spectral leakage is minimized. The vanishing signal amplitude requirement in  $B^2R^2$  and LASSO- $B^2R^2$  may require long observation time to estimate the modulo residue samples. The computational complexities of these algorithms grow fast with the observation length. In contrast, the proposed algorithm follows the principle of STFT and the observation length of a segment can be controlled. That is, we can either choose to unfold few overlapping segments with large observation length or many overlapping segments with small observation length. In addition, the sliding DFT approach enables processing of modulo samples in short frames. This is suitable for real-time applications with low latency requirement.

Our objective is to derive MSE performance guarantees for this recovery scheme and demonstrate the advantage of modulo ADCs which uses the proposed recovery scheme over conventional ADCs. In the next section, the main results of our paper are presented.

## III. PERFORMANCE GUARANTEES USING THE PROPOSED RECOVERY PROCEDURE

### A. Measuring Recovery Performance

Our primary measure of recovery performance of the unfolding scheme is the MSE between the (sampled) input signal  $f[n]$  and the  $\hat{f}[n]$ , given by

$$\begin{aligned}
\text{MSE} &= \frac{1}{N} \sum_{n=0}^{N-1} \mathbb{E} \left\{ |\hat{f}[n] - f[n]|^2 \right\} \\
&= \frac{1}{NI} \sum_{i=1}^I \sum_{n=0}^{N-1} \mathbb{E} \left\{ |\hat{f}^{(i)}[n] - f^{(i)}[n]|^2 \right\} \\
&= \frac{1}{NI} \sum_{i=1}^I \sum_{n=0}^{N-1} \left| \left\{ z^{(i)}[n] - \hat{z}^{(i)}[n] \right\}_{\text{LPF}} \right|^2 \\
&\quad + 2\mathbb{E} \left\{ \epsilon_{\text{LPF}}^{(i)}[n] \right\} \left\{ z^{(i)}[n] - \hat{z}^{(i)}[n] \right\}_{\text{LPF}} \\
&\quad + \mathbb{E} \left\{ |\epsilon_{\text{LPF}}^{(i)}[n]|^2 \right\} \\
&= \frac{1}{NI} \sum_{i=1}^I \sum_{n=0}^{N-1} \left| \left\{ z^{(i)}[n] - \hat{z}^{(i)}[n] \right\}_{\text{LPF}} \right|^2 \\
&\quad + \mathbb{E} \left\{ |\epsilon_{\text{LPF}}^{(i)}[n]|^2 \right\}. \tag{11}
\end{aligned}$$

The second lines comes from partitioning the original signal into  $I$  length- $N$  segments. The third line follows from the expression of the unfolded signal in equation (10) and from

doing some algebraic manipulation. The fourth line comes from the fact that the quantization noise has zero mean. Thus, the second term in the third line can be removed.

From equation (11), it can be seen that the MSE expression comes from two sources: (1) the error due to the modulo residue estimation error and (2) the in-band quantization noise. Our objective in this section is to derive the exact MSE expression as a function of OF and  $b$  when our proposed recovery procedure is used.

### B. Statistical Model for Quantization Noise

Since MSE involves the mean square of the quantization noise, it is crucial to understand the statistical properties of the quantization noise. The statistical nature of the quantization noise comes from the dithered quantization framework established in [32]. This framework is appropriate for the modulo ADC since the folding operation ensures that the signal does not overload the quantizer. The ‘no overloading’ property of the modulo ADC, together with the triangle dither  $d[n]$ , guarantees that the quantization noise is a white process and its power does not depend on the input, i.e.  $\mathbb{E} \{ |\epsilon[n]|^2 | f_{\mathcal{X}}[n] \} = \mathbb{E} \{ |\epsilon[n]|^2 \}$  (see [32, Theorem 2]). For triangle dither  $d[n]$  described in Section II, the induced quantization noise has power  $\mathbb{E} \{ |\epsilon[n]|^2 \} = \frac{1}{4} \left( \frac{2\lambda}{2^b} \right)^2 = \frac{\lambda^2}{2^{2b}}$ .

### C. Incorporating Spectral Leakage

Since spectral leakage cannot be neglected for small  $N$ , we account for the impact of spectral leakage width  $\Omega_{\text{SL}}$  in the proposed recovery algorithm. To this end, we define a quantity  $K_{\text{SL}} = \frac{\Omega_{\text{SL}} \cdot N}{\pi}$  called the *spectral leakage bin count* that corresponds to the number of discrete frequencies in  $(\rho\pi, \rho\pi + \Omega_{\text{SL}}) \cup (2\pi - \rho\pi - \Omega_{\text{SL}}, 2\pi - \rho\pi)$ . This spectral leakage bin count will appear in the derived MSE performance guarantee. Our goal is to identify how our derived performance guarantee maybe affected by this spectral leakage bin count.

### D. Main Result

Before we state the main result of this paper, a proposition about the matrix  $\mathbf{V}_{\mathcal{S}_i}$  is first presented. This will play a key role in the derivation of the main result.

**Proposition 1.** *Let  $f(t)$  be a bandlimited function. The matrices  $\{\mathbf{V}_{\mathcal{S}_i}\}_i$  used in the recovery algorithm have full column rank if*

$$\text{OF} \geq \frac{N}{N - \max_i |\mathcal{S}_i| - K_{\text{SL}}}. \tag{12}$$

*Proof.* See Appendix A.  $\square$

With  $\mathbf{V}_{\mathcal{S}_i}$  being full column rank,  $\mathbf{V}_{\mathcal{S}_i}^\dagger \mathbf{V}_{\mathcal{S}_i}$  is an  $|\mathcal{S}_i| \times |\mathcal{S}_i|$  identity matrix. Under a ‘no quantization noise setting’,  $\|\underline{\mathbf{z}}_{\mathcal{S}_i} - \underline{\mathbf{z}}_{\mathcal{S}_i}\|_\infty = \|\mathbf{V}_{\mathcal{S}_i}^\dagger \mathbf{V}_{\mathcal{S}_i} \underline{\mathbf{z}}_{\mathcal{S}_i} - \underline{\mathbf{z}}_{\mathcal{S}_i}\|_\infty = 0$ . Thus, the full column rank property is crucial for the recovery of  $z^{(i)}[n]$ .

One key observation to note in Proposition 1 is that the oversampling factor OF approaches to unity if  $|\mathcal{S}_i|$  grows strictly slower with  $N$ . This is true for finite-energy bandlimited functions due to their time-domain decay property (see

[8], [9]). That is,  $\exists n_0$  such that  $f[n] < \lambda'$  for all  $n > n_0$ . Consequently,  $\exists N_0$  such that  $|\mathcal{S}_i|$  does not change  $\forall N > N_0$ . Thus, the sampling rate can be made closer to the Nyquist rate for finite-energy bandlimited signals at the expense of longer observation window.

One drawback of Proposition 1 is that it depends on the input signal  $f(t)$ . The following proposition provides a sufficient condition for OF that depends only on the maximum amplitude  $\|f(t)\|_\infty$  and not on the whole  $f(t)$ .

**Proposition 2.** *The matrices  $\{\mathbf{V}_{\mathcal{S}_i}\}_i$  used in the recovery algorithm have full column rank if*

$$\text{OF} \geq \frac{3}{1 - \frac{K_{\text{SL}}}{N}}. \quad (13)$$

This is achieved by setting the modulo threshold to

$$\lambda' = \frac{\|f(t)\|_\infty}{\text{OF} \cdot \left[1 - \frac{K_{\text{SL}}}{N}\right] - 2}. \quad (14)$$

*Proof.* See Appendix B.  $\square$

Note that Proposition 2 is a sufficient but not a necessary condition. We remove the dependence on  $f(t)$  by bounding  $\max_i |\mathcal{S}_i|$  with [9, Equation 14]. However, this bound can be loose in some cases as demonstrated in [9, Table 1].

For  $N$  approaching infinity, equation (13) simplifies to  $\text{OF} \geq 3$ , which was derived in [10]. The theoretical MSE guarantee established in [10] did not take into account the spectral leakage. As demonstrated in Proposition 2, the spectral leakage bin count  $K_{\text{SL}}$  increases the required OF to satisfy condition (13). Nonetheless, its effect on the OF sufficient condition diminishes fast as  $N$  grows.

We can now state the main theoretical result of this paper. The following theorem establishes the MSE of the proposed recovery method when the parameters OF and  $b$  are above certain values.

**Theorem 1.** *Suppose*

$$\text{OF} \geq \frac{3}{1 - \frac{K_{\text{SL}}}{N}} \quad (15)$$

and

$$b > 3 + \log_2 \left(1 + \frac{3M}{4}\right), \quad (16)$$

where  $M = \max_i \|\mathbf{V}_{\mathcal{S}_i}^\dagger \mathbf{V}_{\mathcal{S}_i}\|_\infty$ . The MSE incurred by the proposed recovery algorithm can be written as

$$\text{MSE} = \frac{\|f(t)\|_\infty^2 \left(1 + \frac{K_{\text{SL}}}{N} \cdot \text{OF}\right)}{\text{OF} \cdot (2^b - 2)^2 \cdot \left(\text{OF} \left[1 - \frac{K_{\text{SL}}}{N}\right] - 2\right)^2}. \quad (17)$$

This is achieved by setting the modulo threshold to

$$\lambda' = \frac{\|f(t)\|_\infty}{\text{OF} \cdot \left[1 - \frac{K_{\text{SL}}}{N}\right] - 2}. \quad (18)$$

*Proof.* See Appendix C.  $\square$

The intuition behind the result is that the range of OF and  $b$  in Theorem 1 guarantees that the bounded noise added to the modulo residue pre-estimate  $\tilde{z}^{(i)}[n]$  is within  $(-\lambda', +\lambda')$ . Since  $\tilde{z}^{(i)}[n]$  are integer multiples of  $2\lambda'$ , the rounding

operation maps all modulo residue pre-estimates  $\tilde{z}^{(i)}[n]$  to the correct modulo residue  $z^{(i)}[n]$ . Consequently, only the quantization noise power term in equation (11) appears in the MSE expression.

Our result points out an error in [10, Theorem 1]. The derivation of [10, Theorem 1] did not take into account the contribution of the  $\epsilon^{(i)}[n]$  for  $n \in \mathcal{S}_i^c$ , resulting in  $b > 3$  condition. In our Theorem 1, the second term in equation (16) accounts for the impact of  $\epsilon_{\mathcal{S}_i^c}^{(i)}[n]$  on the recovery performance. Although we are interested in the modulo residue samples located at  $\mathcal{S}_i$ ,  $\epsilon_{\mathcal{S}_i^c}^{(i)}[n]$  still contributes to  $\hat{z}^{(i)}[n]$  through the computation of  $\hat{F}_{\text{OOB}}(e^{j\frac{2\pi k}{N}})$ . In Section IV, we investigate how the second term of (16) is affected by parameters such as segment length, cardinality of  $\mathcal{S}_i$ , and oversampling factor.

It is also important to point out the detrimental impact of spectral leakage bin count to the MSE performance. Neglecting spectral leakage, equation (17) simplifies to

$$\text{MSE} = \frac{\|f(t)\|_\infty^2}{\text{OF} \cdot (2^b - 2)^2 \cdot (\text{OF} - 2)^2}, \quad (19)$$

which exhibits an asymptotic growth rate of  $\mathcal{O}\left(\frac{1}{\text{OF}^3}\right)$ . This is similar to the asymptotic growth rate established in [10] which neglected spectral leakage. When  $K_{\text{SL}} > 0$ , the asymptotic growth rate of the MSE becomes  $\mathcal{O}\left(\frac{1}{\text{OF}^2}\right)$  only. The  $\mathcal{O}\left(\frac{1}{\text{OF}^3}\right)$  growth rate of equation (17) can be maintained if we set  $N \geq \text{OF}$ . However, using a larger window length increases the computational complexity of the sliding window DFT (see Section III-F).

### E. Comparison with Existing Recovery Methods and Conventional ADCs

We now compare the derived theoretical results with other performance guarantees derived for modulo sampling. One popular recovery procedure is the higher-order differences (HoD) approach developed in [6]. Performance guarantee for this algorithm under a bounded noise setting (e.g., quantization noise) has been analyzed in [6, Theorem 6]. More precisely, they showed that for finite-energy bandlimited signals, the noisy unfolded samples can be recovered from noisy modulo samples up to an unknown additive constant, i.e.,

$$\hat{f}_{\text{HoD}}[n] = f[n] + \epsilon[n] + 2\lambda'p,$$

where  $p \in \mathbb{Z}$  is not known, if the sampling rate is at least  $2^\alpha \pi e \times f_{\text{Nyq}}$ . Here,  $\alpha \in \mathbb{N}$  is a parameter of the bounded noise and depends on both the maximum amplitude of the noise and the modulo threshold. In contrast, Theorem 1 only requires  $\text{OF} \geq 3$  under negligible spectral leakage.

A prediction-based approach [12] showed that OF can be made arbitrarily close to unity in exchange for a significant increase in prediction filter length. However, it was pointed out in [12, Section III] that their proposed approach “*collapses in the presence of quantization noise*”. In contrast, our algorithm can work with finite quantization bits. It should also be noted that our proposed algorithm can work at a sampling rate arbitrarily close to the Nyquist rate for finite-energy bandlimited signals and sufficiently large window length  $N$  by virtue of Proposition 1.

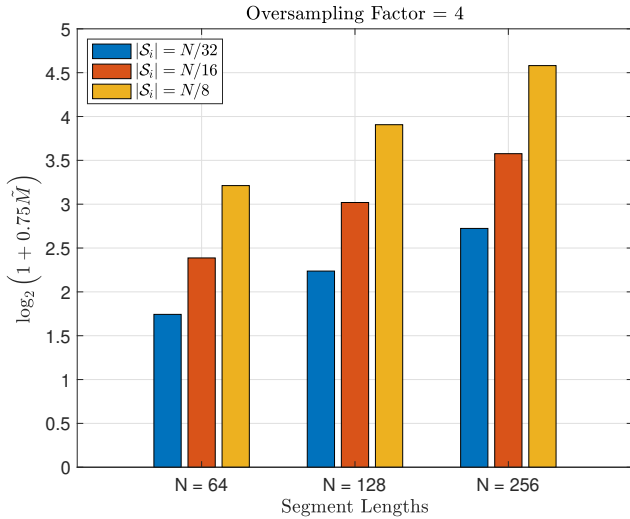


Fig. 4. Empirical evaluation of  $\log_2(1 + 0.75M)$  as a function of segment length ( $N$ ) and  $|S_i|$  for OF = 4.

To demonstrate the advantage of a modulo ADC with 1-bit folding side information over a conventional ADC, we first derive the MSE of a conventional  $b$ -bit ADC under the non-subtractive dithered quantization framework. For a triangle dither  $d[n] \in (-\frac{2\lambda}{2^b}, +\frac{2\lambda}{2^b})$ , the ADC parameter  $\lambda$  should be set to  $\lambda = (1 + \frac{1}{2^b}) \|f(t)\|_\infty$ . After digital filtering, the quantization noise power (which is also the MSE) becomes

$$\text{MSE}_{\text{conv}} = \frac{\|f(t)\|_\infty^2}{\text{OF}(2^b - 2)^2}. \quad (20)$$

Comparing the MSE guarantee for modulo ADC in Theorem 1 and the derived MSE for a conventional ADC, it can be observed that  $\text{MSE}_{\text{mod}} = \mathcal{O}(\frac{1}{\text{OF}^2})$  while  $\text{MSE}_{\text{conv}} = \mathcal{O}(\frac{1}{\text{OF}})$  under sufficiently large  $b$ . The fast decay rate of  $\text{MSE}_{\text{mod}}$  with respect to OF is due to the reduction of the ADC parameter  $\lambda$ . Smaller ADC range entails smaller quantization bins. This demonstrates the superior performance of modulo ADCs over conventional ADCs in oversampled systems.

### F. Computational Complexity

We now derive the computational complexity of the proposed algorithm in terms of the signal length  $N_0$ , window length  $N$ , and window roll-off  $\alpha$  ( $0 \leq \alpha \leq 1$ ). The number of segments depends on the ratio  $\frac{N_0}{N}$ , and the parameter  $\alpha$  dictates how large is the overlap between consecutive segments. For large  $N_0$ , the number of segments to be processed by the algorithm is in  $\mathcal{O}(\frac{N_0}{N(1-\alpha/2)})$ . Looking at the complexity of the residual recovery algorithm at each frame, the calculation of  $\mathbf{V}_{S_i}^\dagger$  is the most computationally-expensive operation. More precisely, this calculation is in  $\mathcal{O}(N^3)$ . Considering all the segments to be processed, the overall computational complexity of the proposed recovery method is in  $\mathcal{O}(\frac{N_0 N^2}{1-\alpha/2})$ .

Based on the derived computational complexity of the proposed algorithm, the speed of the proposed sliding DFT-based recovery scheme can be improved by choosing a small window length. However, a small window length also needs

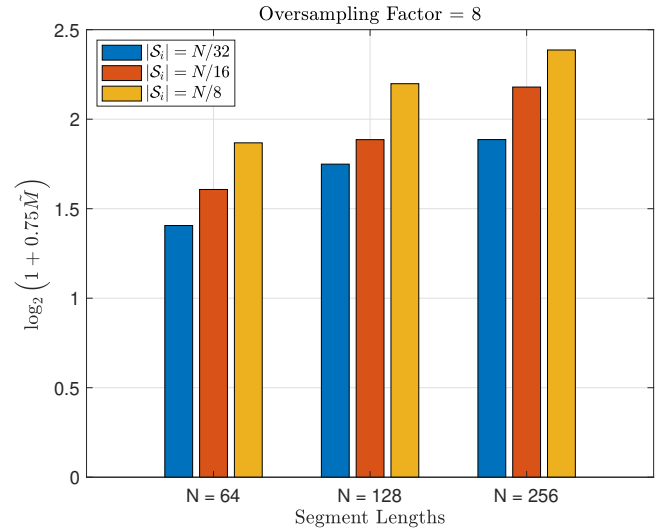


Fig. 5. Empirical evaluation of  $\log_2(1 + 0.75M)$  as a function of segment length ( $N$ ) and  $|S_i|$  for OF = 8.

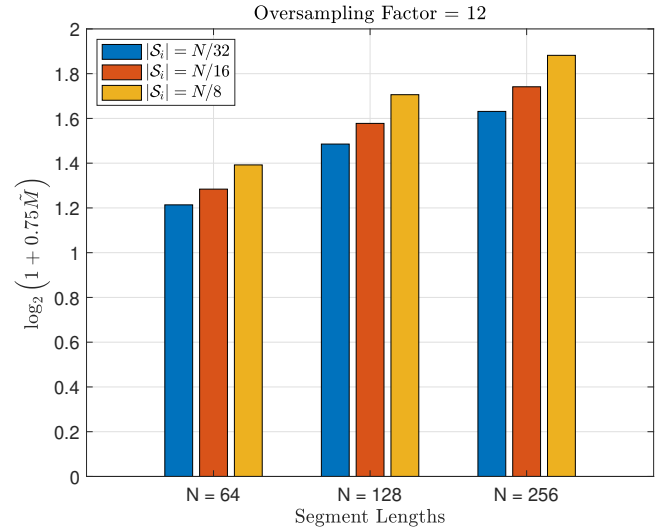


Fig. 6. Empirical evaluation of  $\log_2(1 + 0.75M)$  as a function of segment length ( $N$ ) and  $|S_i|$  for OF = 12.

a higher  $\alpha$  to compensate for the increased spectral leakage. We also note that the recovery algorithm in [10] is a special case of our proposed recovery algorithm with  $N = N_0$  and  $\alpha = 0$ , i.e., rectangular window with no overlap. Hence, its complexity is in  $\mathcal{O}(N_0^3)$ . Since  $N$  is typically chosen to be much smaller than  $N_0$ , our proposed sliding DFT-based recovery is  $\mathcal{O}(\frac{N_0^2(1-\alpha/2)}{N^2})$  faster than the recovery algorithm in [10].

## IV. NUMERICAL RESULTS

In this section, we validate the MSE performance guarantees for the proposed algorithm established in the previous section by comparing the theoretical MSE results with the simulated performance. Numerical experiments are also conducted to

gain additional insight on how the algorithm parameters affect the performance guarantees.

#### A. Analysis of the sufficient condition for $b$

We first investigate how the sufficient condition on  $b$  (i.e., equation (16)) is affected by algorithm and input signal parameters such as segment length  $N$ , oversampling factor OF, and number of non-zero elements of the 1-bit folding information signal  $c[n]$ . To this end, we consider three OF parameter settings (OF = 4, 8, 12) and three segment lengths ( $N = 64, 128, 256$ ). We also consider three values of  $|\mathcal{S}_i|$  ( $|\mathcal{S}_i| = \frac{N}{32}, \frac{N}{16}, \frac{N}{8}$ ). For each combination of these parameter settings, we generate 100,000 realizations of  $\mathbf{V}_{\mathcal{S}_i}$  by selecting  $|\mathcal{S}_i|$  out of  $N$  columns of  $\mathbf{V}$ . We then estimate the second term of equation (16) by calculating

$$\tilde{M} = \max_{i \in \{1, 2, \dots, 100,000\}} \|\mathbf{V}_{\mathcal{S}_i}^\dagger \mathbf{V}_{\mathcal{S}_i} c\|_\infty, \quad (21)$$

where the index  $i$  iterates over all 100,000 random realizations of  $\mathbf{V}_{\mathcal{S}_i}$ .

Figures 4-6 depict the empirical evaluation of  $\log_2(1 + 0.75\tilde{M})$  for OF = 4, OF = 8, and OF = 12, respectively. This term accounts for the extra bit resolution needed by the proposed algorithm (in addition to the 3 bits in the first term of equation (16)) to satisfy the sufficient condition. Based on these evaluations, it can be seen that using a higher oversampling factor generally decreases the second term of equation (16). One insight that can be drawn from this observation is that a reduction in the modulo ADC resolution can be compensated by oversampling. Figures 4-6 also show that longer segment length and frequent crossing of the modulo thresholds increase  $\tilde{M}$ .

As a final note in this numerical experiment, the sufficient condition for  $b$  derived in the previous section may not be tight. We show in the succeeding numerical experiment that the proposed algorithm can achieve the performance guarantees in Theorem 1 even if we set  $b = 4$ .

#### B. Theoretical vs. simulated MSE of the sliding DFT unfolding

To demonstrate the validity of the theoretical MSE guarantees, we consider the input signal

$$f(t) = \sum_{m=1}^{100,000} A_m \cdot p_{rc}(t - mT), \quad (22)$$

where  $p_{rc}(t)$  is a raised-cosine pulse with roll-off parameter  $\beta = 1$ . The peak amplitude of the raised-cosine pulse  $p_{rc}(t)$  is set to unity. The pulse amplitude  $A_m$  is drawn uniformly from the discrete set  $\{-2, -1, 0, +1, +2\}$ , and  $T$  is the time difference between two consecutive pulses. Intuitively, the signal  $f(t)$  is constructed by generating 100,000 raised-cosine pulses with random amplitudes at every symbol period  $T$ . This signal is fed to a low-resolution 4-bit modulo ADC with sampling rate  $\frac{1}{T_s} = \frac{\text{OF}\omega_m}{2\pi}$  to produce the quantized modulo samples  $f_{\mathcal{X},q}[n]$ . The dither sequence and modulo threshold are configured according to the modulo ADC parameters.

For the sliding DFT-based recovery algorithm, we set the roll-off parameter of the tapered cosine window to  $\alpha = 0.25$

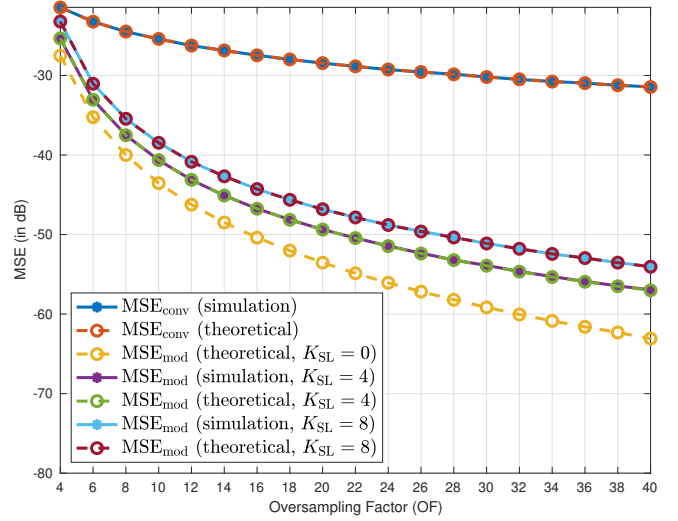


Fig. 7. Simulated and theoretical MSE vs. oversampling factor of the proposed sliding DFT-based unfolding algorithm for  $N = 64$ ,  $\alpha = 0.25$ , and  $K_{\text{SL}} = 4, 8$ . Superimposed in the figure are the simulated and theoretical MSE curves of a conventional ADC.

and window length  $N = 64$ . Note that the length of the tapered cosine window is also the segment length and the DFT size of the algorithm. To investigate the impact of spectral leakage, we consider two different spectral leakage bin counts:  $K_{\text{SL}} = 4, 8$ . The simulated performance is evaluated by taking the squared difference between the true samples  $f[n]$  and the signal unfolding output  $\hat{f}[n]$  and averaging the results over all  $n$ .

Figure 7 depicts the simulated MSE (in decibels) of the modulo ADC with sliding DFT recovery and its the theoretical MSE (based on Theorem 1) under the aforementioned settings. The oversampling factor is swept from OF = 4 to OF = 40. The numerical results for modulo ADC demonstrate that the derived MSE performance guarantee is accurate since it coincides with the simulated MSE for all OF and  $K_{\text{SL}}$  settings considered. It can be observed that larger  $K_{\text{SL}}$  increases the MSE of the sliding DFT unfolding method. This can be attributed to the widening of the passband region of the digital LPF used in the last step of the unfolding method. Consequently, more quantization noise are able to pass through the digital LPF.

The theoretical MSE curve for  $K_{\text{SL}} = 0$  (i.e. spectral leakage neglected) is also superimposed in Figure 7. It is evident from the figure that the slope of the  $K_{\text{SL}} = 0$  MSE curve is steeper at the high OF regime compared to those of  $K_{\text{SL}} = 4$  and  $K_{\text{SL}} = 8$  MSE curves. This validates the asymptotic MSE growth rates mentioned in Section III. Nonetheless, the modulo ADC which uses our sliding DFT recovery still outperforms the conventional ones even if there is spectral leakage. The gap between the MSE curves of the modulo ADC and conventional ADC widens as OF is increased.



## V. SUMMARY AND FUTURE DIRECTIONS

In this work, we considered a modulo ADC system in which the output samples are associated with a 1-bit folding information signal  $c[n]$ . The unfolded samples are obtained using the sliding DFT-based recovery scheme described in Section II-C. The advantage of our proposed unfolding scheme over existing Fourier-based recovery algorithms for modulo sampling is the significant reduction in the length of the observation window. This reduction in the observation time has a positive impact in the algorithm's computational complexity. We also provide sufficient conditions on the oversampling factor and ADC resolution to attain a certain MSE performance guarantee. When these sufficient conditions are met, the MSE performance of the modulo ADC which uses our proposed recovery method is better compared to that of conventional ADCs. Moreover, we also showed that spectral leakage affects the asymptotic MSE growth rate of our sliding DFT recovery method. These theoretical results are substantiated by the numerical experiments conducted in Section IV.

It is worth mentioning that while the proposed unfolding scheme relies on the availability of 1-bit folding information signal  $c[n]$ , the proposed recovery can be modified to work without  $c[n]$ . This can be done by performing support recovery on  $\tilde{z}_w^{(i)}[n]$ . This idea, together with its performance guarantees, is considered a potential subject of future work. We also note that the sufficient conditions derived for the oversampling factor and ADC resolution are not tight. Hence, another future direction is to tighten these sufficient conditions. Lastly, it is also of interest to apply this proposed recovery algorithm to specific low-resolution signal processing systems (e.g., communication receivers, radars, etc.).

### APPENDIX A PROOF OF PROPOSITION 1

A necessary condition for  $\mathbf{V}_{\mathcal{S}_i}$  to be full column rank is  $|\mathcal{S}_i| \leq K$ . Since the columns of  $\mathbf{V}_{\mathcal{S}_i}$  are derived from the columns of the Fourier basis, they are linearly independent. Thus, the condition  $|\mathcal{S}| \leq K$  is also sufficient. The number of discrete frequencies in the out-of-band region can be lower bounded by

$$\begin{aligned} K &= N - 2 \left\lfloor \frac{\rho K}{2} \right\rfloor - K_{\text{SL}} \\ &\geq N(1 - \rho) - K_{\text{SL}}. \end{aligned} \quad (23)$$

To establish  $|\mathcal{S}_i| \leq K$ , it suffices to show that

$$|\mathcal{S}_i| \leq N(1 - \rho) - K_{\text{SL}}$$

or, equivalently,

$$\text{OF} \geq \frac{N}{N - |\mathcal{S}_i| - K_{\text{SL}}}. \quad (24)$$

Here, we used  $\text{OF} = \frac{1}{\rho}$ . The proof is completed by taking the maximum over all  $|\mathcal{S}_i|$ .

### APPENDIX B PROOF OF PROPOSITION 2

Our starting point is the result in Proposition 1:

$$\text{OF} \geq \frac{N}{N - \max_i |\mathcal{S}_i| - K_{\text{SL}}}. \quad (25)$$

We bound the size of  $\mathcal{S}_i$  using an expression that is independent of the segment index. Our bound on  $|\mathcal{S}_i|$  is based on [9, Equation 14]:

$$\begin{aligned} |\mathcal{S}_i| &\leq 4 \left\lfloor \frac{\rho N}{2} \right\rfloor + 4 \left\lfloor \frac{\rho N}{2} \right\rfloor \cdot \left\lfloor \frac{\|f(t)\|_\infty - \lambda'}{2\lambda'} \right\rfloor \\ &\leq 2\rho N + 2\rho N \cdot \left( \frac{\|f(t)\|_\infty - \lambda'}{2\lambda'} \right) \end{aligned} \quad (26)$$

for all  $i$ , where second inequality comes from the trivial lower bound of the floor function, i.e.,  $\lfloor x \rfloor \geq x$ . Since the bound in equation (26) is independent of  $i$ , this bound is also an upper bound for  $\max_i |\mathcal{S}_i|$ . By replacing  $\max_i |\mathcal{S}_i|$  in equation (25) with its upper bound in equation (26) and by doing some algebraic manipulation, we get

$$\text{OF} \geq \frac{\frac{\|f(t)\|_\infty}{\lambda'} + 2}{1 - \frac{K_{\text{SL}}}{N}}. \quad (27)$$

Using

$$\lambda' = \frac{\|f(t)\|_\infty}{\text{OF} \cdot \left[ 1 - \frac{K_{\text{SL}}}{N} \right] - 2}$$

as the modulo threshold for equation (27) gives us  $\text{OF} \geq 3$ . However, since  $\lambda' \leq \|f(t)\|_\infty$ , then

$$\text{OF} \cdot \left[ 1 - \frac{K_{\text{SL}}}{N} \right] - 2 > 1.$$

This implies that

$$\text{OF} \geq \frac{3}{1 - \frac{K_{\text{SL}}}{N}}$$

must also hold. The OF requirements are satisfied simultaneously if equation (13) holds.

### APPENDIX C PROOF OF THEOREM 1

As an initial step, an  $\ell_\infty$ -norm bound on the difference between the modulo residue pre-estimate  $\tilde{\mathbf{z}}$  and modulo residue  $\mathbf{z}$  is established:

$$\begin{aligned} \|\tilde{\mathbf{z}} - \mathbf{z}\|_\infty &= \|\tilde{\mathbf{z}}_{\mathcal{S}_i} - \mathbf{z}_{\mathcal{S}_i}\|_\infty \\ &= \|\mathbf{V}_{\mathcal{S}_i}^\dagger \hat{\mathbf{F}}_{\text{OOB}} - \mathbf{z}_{\mathcal{S}_i}\|_\infty \\ &= \|\mathbf{V}_{\mathcal{S}_i}^\dagger \mathbf{V}_{\mathcal{S}_i} (\mathbf{z}_{\mathcal{S}_i} + \underline{\boldsymbol{\epsilon}}_{\mathcal{S}_i}) + \mathbf{V}_{\mathcal{S}_i}^\dagger \mathbf{V}_{\mathcal{S}_i^c} \underline{\boldsymbol{\epsilon}}_{\mathcal{S}_i^c} - \mathbf{z}_{\mathcal{S}_i}\|_\infty \\ &= \|\mathbf{V}_{\mathcal{S}_i}^\dagger \mathbf{V} \underline{\boldsymbol{\epsilon}}\|_\infty \\ &\leq \left( 1 + \|\mathbf{V}_{\mathcal{S}_i}^\dagger \mathbf{V}_{\mathcal{S}_i^c}\|_\infty \right) \cdot \|\underline{\boldsymbol{\epsilon}}\|_\infty \\ &\leq \left( 1 + \|\mathbf{V}_{\mathcal{S}_i}^\dagger \mathbf{V}_{\mathcal{S}_i^c}\|_\infty \right) \cdot \left( \frac{6\lambda}{2^b} \right) \\ &= \left( 1 + \|\mathbf{V}_{\mathcal{S}_i}^\dagger \mathbf{V}_{\mathcal{S}_i^c}\|_\infty \right) \cdot \left( \frac{6\lambda'}{2^b - 2} \right). \end{aligned}$$

The first line comes from the fact that  $\tilde{z}^{(i)}[n] = z^{(i)}[n] = 0$  for  $n \notin \mathcal{S}_i$ . The second and third lines come from equations (6) and (7). Because the last  $\frac{\alpha N}{2}$  samples of  $\tilde{z}_w^{(i-1)}[n]$  is added to the first  $\frac{\alpha N}{2}$  samples of  $\tilde{z}_w^{(i)}[n]$ , the effect of the window function is removed. Consequently, the subscript  $w$  is dropped in the second line. The fourth line holds because  $\mathbf{V}_{\mathcal{S}_i}$  is full column rank by Proposition 2 and  $\mathbf{V}_{\mathcal{S}_i}^\dagger \mathbf{V}_{\mathcal{S}_i} \boldsymbol{\epsilon}_{\mathcal{S}_i} + \mathbf{V}_{\mathcal{S}_i}^\dagger \mathbf{V}_{\mathcal{S}_i^c} \boldsymbol{\epsilon}_{\mathcal{S}_i^c} = \mathbf{V}_{\mathcal{S}_i}^\dagger \mathbf{V} \boldsymbol{\epsilon}$ . The fifth line follows from the property  $\|\mathbf{A}\mathbf{x}\|_\infty \leq \|\mathbf{A}\|_\infty \|\mathbf{x}\|_\infty$ . The sixth line holds because the triangle dither induces a quantization noise  $\epsilon[n]$  whose range of amplitude is  $(-\frac{3\lambda}{2b}, +\frac{3\lambda}{2b})$ . Consequently,  $\epsilon[n]$  has amplitude in  $(-\frac{6\lambda'}{2b}, +\frac{6\lambda'}{2b})$ . Finally, the last line comes from the relationship between the modulo threshold  $\lambda'$  and the ADC dynamic range parameter  $\lambda$ .

Suppose we let  $M = \max_i \|\mathbf{V}_{\mathcal{S}_i}^\dagger \mathbf{V}_{\mathcal{S}_i^c}\|_\infty$ . The first-order difference of the pre-estimate  $\tilde{z}^{(i)}[n]$  is at most  $\frac{6\lambda'}{2b-2}(1+M)$  away from the first-order difference of the true residue sample. Since a rounding operation to the nearest integer multiple of  $2\lambda'$  is applied to the  $\tilde{z}^{(i)}[n]$  to get  $\hat{z}^{(i)}[n]$ , perfect recovery of  $z^{(i)}[n]$  after the application of the rounding operation and equation (9) is guaranteed if

$$\frac{6\lambda'}{2b-2}(1+M) < \lambda',$$

or equivalently,

$$3 + \log_2 \left( 1 + \frac{3}{4}M \right) < b.$$

This is satisfied by the assumption on  $b$  stated in the theorem.

With perfect recovery of the  $z^{(i)}[n]$ , the terms  $|z^{(i)}[n] - \hat{z}^{(i)}[n]| = 0$  for all  $i$  and  $n$ . Thus, the MSE is solely due to the quantization noise power after filtering. From Section III-B, the quantization noise power is  $\mathbb{E}\{|\epsilon[n]|^2\} = \frac{1}{4}(\frac{2\lambda}{2b})^2$ . This quantization noise power is spread evenly over the entire bandwidth  $(-\pi, \pi)$  since  $\epsilon[n]$  is a white process. Considering the filtering operation via a digital LPF with passband region  $(-\frac{\pi}{\text{OF}} - \Omega_{\text{SL}}, +\frac{\pi}{\text{OF}} + \Omega_{\text{SL}})$  after the unfolding step, the power of the filtered quantization noise is only  $\frac{1 + \frac{K_{\text{SL}}}{N} \cdot \text{OF}}{\text{OF}}$  of  $\mathbb{E}\{|\epsilon^{(i)}[n]|^2\}$ :

$$\begin{aligned} \mathbb{E}\left\{|\epsilon_{\text{LPF}}^{(i)}[n]|^2\right\} &= \frac{\mathbb{E}\{|\epsilon^{(i)}[n]|^2\}}{\text{OF}} \left(1 + \frac{K_{\text{SL}}}{N} \cdot \text{OF}\right) \\ &= \frac{\lambda^2}{\text{OF} \cdot 2^{2b}} \left(1 + \frac{K_{\text{SL}}}{N} \cdot \text{OF}\right) \\ &= \frac{(\lambda')^2}{\text{OF} \cdot (2^b - 2)^2} \left(1 + \frac{K_{\text{SL}}}{N} \cdot \text{OF}\right). \end{aligned}$$

The proof is completed by setting  $\lambda' = \frac{\|f(t)\|_\infty}{\text{OF} \cdot \left[1 - \frac{K_{\text{SL}}}{N}\right] - 2}$ .

## REFERENCES

- [1] Y. C. Eldar, *Sampling Theory: Beyond Bandlimited Systems*. Cambridge University Press, 2015.
- [2] C. Shannon, "Communication in the presence of noise," *Proceedings of the IRE*, vol. 37, no. 1, pp. 10–21, 1949.
- [3] T. Berger, *Rate Distortion Theory: A Mathematical Basis for Data Compression*. Englewood Cliffs, NJ, USA: Prentice-Hall, 1971.
- [4] R. Walden, "Analog-to-digital converter survey and analysis," *IEEE Journal on Selected Areas in Communications*, vol. 17, no. 4, pp. 539–550, 1999.
- [5] B. Laporte-Fauret, G. Ferré, D. Dallet, B. Minger, and L. Fuché, "Adc resolution for simultaneous reception of two signals with high dynamic range," in *2018 25th IEEE International Conference on Electronics, Circuits and Systems (ICECS)*, 2018, pp. 729–732.
- [6] A. Bhandari, F. Krahmer, and R. Raskar, "On unlimited sampling and reconstruction," *IEEE Transactions on Signal Processing*, vol. 69, pp. 3827–3839, 2021.
- [7] A. Bhandari, F. Krahmer, and T. Poskitt, "Unlimited Sampling From Theory to Practice: Fourier-Prony Recovery and Prototype ADC," *IEEE Trans. Signal Process.*, vol. 70, pp. 1131–1141, 2022.
- [8] E. Azar, S. Mulleti, and Y. C. Eldar, "Robust unlimited sampling beyond modulo," *arXiv preprint arXiv:2206.14656*, 2022.
- [9] S. B. Shah, S. Mulleti, and Y. C. Eldar, "Lasso-based fast residual recovery for modulo sampling," in *ICASSP 2023 - 2023 IEEE International Conference on Acoustics, Speech and Signal Processing (ICASSP)*, 2023, pp. 1–5.
- [10] N. I. Bernardo, S. B. Shah, and Y. C. Eldar, "Modulo sampling with 1-bit side information: Performance guarantees in the presence of quantization," in *2024 IEEE International Symposium on Information Theory (ISIT)*, 2024, pp. 3498–3503.
- [11] M. Beckmann, A. Bhandari, and M. Iske, "Fourier-domain inversion for the modulo radon transform," *IEEE Transactions on Computational Imaging*, vol. 10, pp. 653–665, 2024.
- [12] E. Romanov and O. Ordentlich, "Above the nyquist rate, modulo folding does not hurt," *IEEE Signal Processing Letters*, vol. 26, no. 8, pp. 1167–1171, 2019.
- [13] R. Guo and A. Bhandari, "Iter-sis: Robust unlimited sampling via iterative signal sieving," in *ICASSP 2023 - 2023 IEEE International Conference on Acoustics, Speech and Signal Processing (ICASSP)*, 2023, pp. 1–5.
- [14] O. Musa, P. Jung, and N. Goertz, "Generalized approximate message passing for unlimited sampling of sparse signals," in *2018 IEEE Global Conference on Signal and Information Processing (GlobalSIP)*, 2018, pp. 336–340.
- [15] V. Shah and C. Hegde, "Sparse signal recovery from modulo observations," *EURASIP Journal on Advances in Signal Processing*, vol. 2021, no. 1, pp. 1–17, 2021.
- [16] D. Prasanna, C. Sriram, and C. R. Murthy, "On the identifiability of sparse vectors from modulo compressed sensing measurements," *IEEE Signal Processing Letters*, vol. 28, pp. 131–134, 2021.
- [17] G. Shtendel and A. Bhandari, "Dual-channel unlimited sampling for bandpass signals," in *ICASSP 2024 - 2024 IEEE International Conference on Acoustics, Speech and Signal Processing (ICASSP)*, 2024, pp. 9711–9715.
- [18] S. Mulleti, E. Reznitskiy, S. Savariego, M. Namer, N. Glazer, and Y. C. Eldar, "A hardware prototype of wideband high-dynamic range analog-to-digital converter," *IET Circuits, Devices & Systems*, vol. 17, no. 4, pp. 181–192, 2023.
- [19] A. Krishna, S. Rudresh, V. Shaw, H. R. Sabbella, C. S. Seelamantula, and C. S. Thakur, "Unlimited dynamic range analog-to-digital conversion," 2019.
- [20] O. Ordentlich, G. Tabak, P. K. Hanumolu, A. C. Singer, and G. W. Wornell, "A modulo-based architecture for analog-to-digital conversion," *IEEE Journal of Selected Topics in Signal Processing*, vol. 12, no. 5, pp. 825–840, 2018.
- [21] T. Feuillen, M. Alae-Kerahroodi, A. Bhandari, B. S. M. R, and B. Ottersten, "Unlimited sampling for fmcw radars: A proof of concept," in *2022 IEEE Radar Conference (RadarConf22)*, 2022, pp. 1–5.
- [22] T. Feuillen, B. Shankar MRR, and A. Bhandari, "Unlimited sampling radar: Life below the quantization noise," in *ICASSP 2023 - 2023 IEEE International Conference on Acoustics, Speech and Signal Processing (ICASSP)*, 2023, pp. 1–5.
- [23] Q. Zhang, J. Zhu, Z. Xu, and D. W. Soh, "One-bit-aided modulo sampling for doa estimation," *ArXiv*, vol. abs/2309.04901, 2023. [Online]. Available: <https://api.semanticscholar.org/CorpusID:261681728>
- [24] Z. Liu, A. Bhandari, and B. Clerckx, " $\lambda$ -mimo: Massive mimo via modulo sampling," *IEEE Transactions on Communications*, vol. 71, no. 11, pp. 6301–6315, 2023.
- [25] L. G. Ordoñez, P. Ferrand, M. Duarte, M. Guillaud, and G. Yang, "On full-duplex radios with modulo-adcs," *IEEE Open Journal of the Communications Society*, vol. 2, pp. 1279–1297, 2021.

- [26] G. Shtendel, D. Florescu, and A. Bhandari, "Unlimited sampling of bandpass signals: Computational demodulation via undersampling," *IEEE Transactions on Signal Processing*, vol. 71, pp. 4134–4145, 2023.
- [27] A. Bhandari and F. Kraemer, "Hdr imaging from quantization noise," in *2020 IEEE International Conference on Image Processing (ICIP)*, 2020, pp. 101–105.
- [28] T. Geng, F. Ji, Pratibha, and W. P. Tay, "Modulo eeg signal recovery using transformer," in *ICASSP 2023 - 2023 IEEE International Conference on Acoustics, Speech and Signal Processing (ICASSP)*, 2023, pp. 1–5.
- [29] J. Rhee and Y. Joo, "Wide dynamic range cmos image sensor with pixel level adc," *Electronics Letters*, vol. 39, pp. 360 – 361, 03 2003.
- [30] K. Sasagawa, T. Yamaguchi, M. Haruta, Y. Sunaga, H. Takehara, H. Takehara, T. Noda, T. Tokuda, and J. Ohta, "An implantable cmos image sensor with self-reset pixels for functional brain imaging," *IEEE Transactions on Electron Devices*, vol. 63, no. 1, pp. 215–222, 2016.
- [31] MathWorks. (2024) Tukey window. Accessed: 2024-9-23. [Online]. Available: <https://www.mathworks.com/help/signal/ref/tukeywin.html>
- [32] R. Gray and T. Stockham, "Dithered quantizers," *IEEE Transactions on Information Theory*, vol. 39, no. 3, pp. 805–812, 1993.